ISSN: 1410-8917
Jurnal Kimia Sains & Aplikasi
e-ISSN: 2597-9914

Jurnal Kimia Sains dan Aplikasi 29 (1) (2026): 10-21

Jurnal Kimia Sains dan Aplikasi
Journal of Scientific and Applied Chemistry

Journal homepage: http://ejournal.undip.ac.id/index.php/ksa

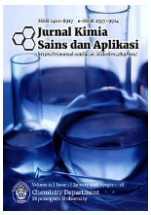

Iron Ion Removal from Water Using Clay Honeycomb Monolith

Darmadi [1], Mirna Rahmah Lubis [1,*], Adisalamun [1], Muhammad Zaki [2]

[1] Chemical Engineering Department, Faculty of Engineering, Universitas Syiah Kuala, Banda Aceh, Indonesia
[2] Process Technology Laboratory, Universitas Syiah Kuala, Banda Aceh, Indonesia

* Corresponding author: mirna@che.usk.ac.id

https://doi.org/10.14710/jksa.29.1.10-21

Article Info

Article history:

Received: 10th July 2025
Revised: 24th December 2025
Accepted: 25th December 2025
Online: 07th February 2026

Keywords:
Adsorption; characterization; clay honeycomb monolith; Fe^{2+} ion; kinetics

Abstract

Groundwater contamination by dissolved iron remains a widespread problem, particularly in decentralized water treatment systems, where simple, hydraulically efficient solutions are required. This study investigates a clay-based honeycomb monolith (CBM) as a structured adsorbent for Fe^{2+} removal from aqueous solutions, with simultaneous evaluation of adsorption and flow performance. The CBM was fabricated from natural clay and characterized using XRD, BET, SEM, and FTIR analyses. Batch adsorption experiments were conducted at Fe^{2+} concentrations of 2–9 mg L^{-1}, and kinetic and isotherm models were applied. In addition, pressure drop measurements were performed under continuous-flow conditions using monoliths of varying heights. The CBM exhibited a specific surface area of 55 m^2 g^{-1} and followed pseudo-second-order kinetics, while equilibrium data were best described by the Langmuir model with a maximum adsorption capacity of 0.229 mg g^{-1}. Importantly, the monolithic structure exhibited low pressure drop (up to 18.54 kPa m^{-1}), significantly lower than that of typical packed beds. The unique contribution of this work is to demonstrate that clay-based honeycomb monoliths can combine adsorption functionality with favorable hydraulic performance, highlighting their potential for practical iron removal in continuous-flow water treatment systems.

1. Introduction

Groundwater is a major source of drinking water worldwide because of its wide availability and relatively low treatment cost [1], particularly in rural and developing regions. However, it frequently contains naturally occurring dissolved iron (Fe^{2+}), which can exceed potable water standards and cause discoloration, metallic taste, corrosion of distribution systems, and interference with disinfection processes. In reducing aquifer environments, iron occurs predominantly as soluble and colorless Fe^{2+}, making its removal particularly challenging. Accordingly, international guidelines such as those of the World Health Organization limit iron concentration to 0.3 mg L^{-1} in drinking water and 1 mg L^{-1} for freshwater systems [2]. Recent studies continue to report elevated dissolved Fe^{2+} levels in groundwater and persistent treatment challenges in decentralized water supplies. Field surveys and reviews report widespread Fe occurrence, seasonal variability linked to redox conditions, and persistent treatment needs in many regions [3].

Conventional removal approaches (oxidation/filtration, ion exchange, membranes, chemical precipitation, electrocoagulation [4]) can be effective but are often limited by high energy use, fouling risk, sludge generation, or the need for complex infrastructure–constraints that reduce their suitability for low-resource or small-scale systems. Membrane-based systems [5] and ion-exchange resins often require high energy input and fouling control, while chemical precipitation and coagulation processes generate sludge that must be treated and disposed of properly. These practical limitations motivate the search for simple, robust adsorbent configurations that perform under continuous-flow conditions [6].

The honeycomb monolith architecture is attractive for such applications because it provides an ordered array of parallel microporous channels that markedly reduce pressure drop and promote uniform flow distribution

compared with packed beds, while also shortening diffusion paths and improving mass transfer coefficients relative to conventional pellet or powder beds. In addition, the monolithic form offers mechanical integrity, avoids powder handling and post-treatment separation (89%) [7], and permits wall-level mesoporosity to supply adsorption sites—an advantageous combination for continuous-flow water treatment [8].

Although clay-based honeycomb monoliths (CBMs) have been explored for water purification and related contaminants (e.g., organics and selected metal ions), and structured monoliths have demonstrated lower hydraulic resistance and improved transport behavior in gas and liquid phase studies, systematic data on Fe^{2+} adsorption in aqueous systems that combine adsorption performance with pressure-drop characterization are still scarce [9]. Unlike powdered or pelletized adsorbents, which often suffer from high pressure drop, channeling, and handling difficulties in fixed-bed systems, honeycomb monoliths provide ordered macroporous channels that promote uniform flow distribution and low hydraulic resistance. The structured architecture enhances mass transfer [10] by minimizing dead volume and promoting uniform flow, while eliminating the need for post-treatment separation of fine particles. The rigid monolithic improves mechanical integrity and eliminates the need for post-treatment [11] solid-liquid separation, while mesoporosity within the monolith walls provides adsorption sites for dissolved species.

Therefore, this study specifically aims to synthesize and characterize a clay-based honeycomb monolith and to evaluate its Fe^{2+} removal performance, adsorption kinetics and isotherms, and pressure-drop behavior under continuous-flow-relevant conditions, thereby addressing the gap between adsorption capacity and hydraulic feasibility for practical groundwater treatment.

2. Experimental

2.1. Materials

A certified iron standard solution (1000 ± 2 ppm, Merck) was used as the Fe^{2+} source. Fe^{2+} working solutions of 2 and 4 mg L^{-1} were prepared by dilution of the standard solution according to Equation 1.

$$M_1 \times V_1 = M_2 \times V_2 \quad (1)$$

Where, V_1 and M_1 denoted the volume and concentration of the stock solution, while V_2 and M_2 referred to the total volume and concentration of the diluted solution. Concentrations were verified by atomic absorption spectroscopy, and the absorbance of the 2 mg L^{-1} solution was measured via Atomic Absorption Spectroscopy (AAS) at 248 nm. The measured concentrations were 1.98 and 3.98 mg L^{-1}, confirming the accuracy of the preparation.

The raw clay used for monolith fabrication was collected from Sigli, Aceh Province, Indonesia. XRD analysis of the calcined clay-based monolith (Figure 3) indicates that quartz (SiO_2) is the dominant crystalline phase (~87.5%), accompanied by minor aluminosilicate phases. No characteristic basal reflections corresponding to kaolinite, montmorillonite, or illite were observed. Accordingly, the material is classified as a quartz-rich natural clay rather than a single clay mineral species.

2.2. Experiment

The raw clay was first cleaned to remove impurities, ground using a ball mill, and sieved through a 100-mesh sieve. A small amount of water was added to obtain a homogeneous plastic paste, which was molded (Figure 1) into honeycomb monoliths with a diameter of 1.5 cm, a height of 1.8 cm, and 37 parallel channels. The resulting monoliths had an average mass of 4.61 g (Figure 2). The molded samples were air-dried for 48 h and subsequently calcined at 600°C for 3 h to improve mechanical stability.

The CBM was characterized using X-ray Diffraction (XRD), Fourier Transform Infrared Spectroscopy (FTIR), Brunauer-Emmet-Teller (BET) surface area analysis, and Scanning Electron Microscopy (SEM).

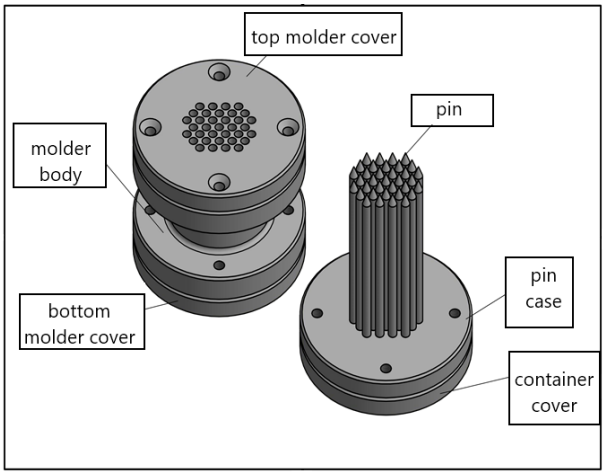

Figure 1. The CBM molder

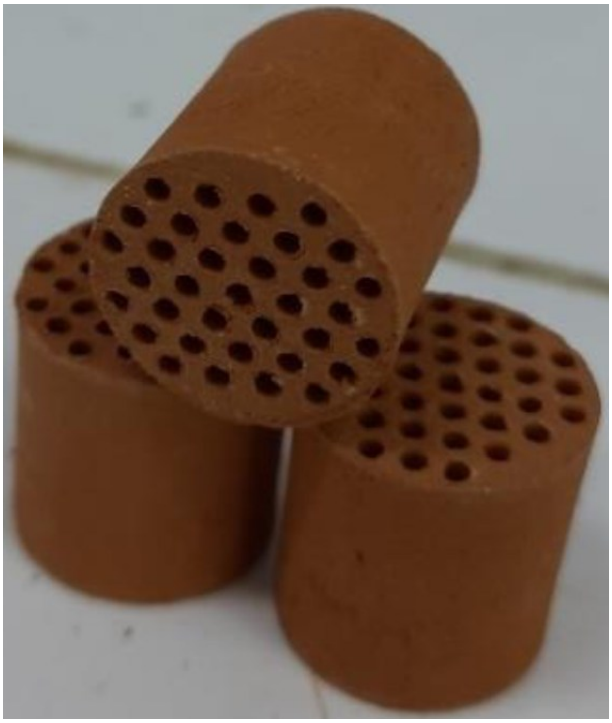

Figure 2. CBM product prepared using the mold method

Specific surface area and pore characteristics were determined by N_2 adsorption-desorption measurement using a BET analyzer (Micromeritics ASAP 2020). Prior to analysis, samples were oven-dried at 110–150°C and degassed under vacuum at 250°C for 2 h. Measurements were performed at 195.8°C over a relative pressure (p/p_0) range of 0.03–0.3. The specific surface area was calculated using the BET method. Mesopore size distribution and pore volume were obtained from the desorption branch of the isotherm using the Barrett-Joyner-Halenda (BJH) method.

Phase identification was performed using an X'Pert3 Powder diffractometer (PANalytical, Netherlands) with Cu Kα radiation (λ = 1.541874 Å). Diffraction data were collected over a 2θ range of 1.914°–89.878°, using a step size of 0.026° and a scan rate of 1.9 min^{-1}. The experimental diffraction pattern was analyzed by comparison with reference data from the Crystallography Open Database (COD-inorg, REV214414, 2019.03.29). Mineral phases were identified by peak-matching, and the corresponding phase assignments are shown in Figure 3.

Pressure-drop measurements were performed in a fixed-bed column using calibrated water pressure installed at the column inlet (P_1) and outlet (P_2). Prior to each experimental run, the pressure sensors were calibrated using a static water column to ensure accurate pressure readings over the measurement range. Calibration was verified before and after the experiments, and deviations were within ±2% of the full-scale reading.

CBM samples were placed in the column at bed heights of 40, 60, and 100 cm, ensuring proper alignment to avoid channeling and non-uniform flow distribution. During each test, water was passed through the column at a constant superficial velocity of 0.1 m s^{-1} under ambient conditions. The pressure drop (ΔP) across the adsorbent bed was calculated as the difference between inlet and outlet pressures according to Equation (2).

$$\Delta P = P_1 - P_2 \quad (2)$$

For each bed height, measurements were repeated three times after steady-state flow was reached, and the reported pressure drop represents the average. The experimental uncertainty was estimated from repeated measurements and sensor accuracy, with an overall uncertainty of less than ±5%.

Batch adsorption measurements were conducted to evaluate Fe^{2+} removal by the CBM. Preliminary kinetic investigations were first performed to determine the equilibrium contact time. In these investigations, CBM samples were contacted with 400 mL of Fe^{2+} solutions (2 and 4 mg L^{-1}) under continuous stirring (110 rpm) at room temperature. Aliquots of 10 mL were withdrawn at predetermined time intervals of 40, 80, 120, 160, 200, and 240 minutes until no significant change in Fe^{2+} concentration was observed. Equilibrium was assumed when the change in Fe^{2+} concentration was less than 5% over two consecutive sampling intervals. The pseudo-first-order and pseudo-second-order models were used to analyze the adsorption data, as shown in Equations (3) and (4).

For pseudo-first-order:

$$q_t = q_e(1 - e^{-k_1 t}) \quad (3)$$

For pseudo-second-order:

$$q_t = \frac{k_2 q_e^2 t}{1 + k_2 q_e t} \quad (4)$$

In these equations, q_t and q_e denote the amount of metal ion adsorbed (mg g^{-1}) at a specific time and at equilibrium, respectively. The rate constant for the pseudo-first-order model was represented by k_1 (min^{-1}), while k_2 (g mg^{-1} min^{-1}) corresponded to the rate constant for the pseudo-second-order model. The adsorption rate kinetics were determined by selecting the smallest difference between the measured and calculated adsorption capacities and the lowest SSE value. Adsorption kinetics and isotherm measurements were conducted as single measurements under controlled conditions. Therefore, statistical error bars are not reported.

Based on these kinetic results, the adsorption equilibrium was reached after 240 min for both initial concentrations. Consequently, all subsequent isotherm investigations were conducted with a contact time of 240 min to ensure equilibrium conditions. The equilibrium adsorption capacity (q_e) was calculated from the difference between the initial and equilibrium Fe^{2+} concentrations. Adsorption isotherms were measured over an initial Fe^{2+} concentration range of 2–9 mg L^{-1}. In this work, isotherms were determined using the Langmuir, Freundlich, and Brunauer–Emmett–Teller (BET) equations. These equations were listed in Equations (5)–(7).

$$q_e = \frac{K_L \times C_e}{1 + a_L \times C_e} \quad (5)$$

$$q_e = K_f \times C_e^{\frac{1}{n}} \quad (6)$$

$$q_e = \frac{qs \times C_{BET} \times C_e}{(C_o - C_e) \times \left[1 + (C_{BET} - 1) \times \left(\frac{C_e}{C_o}\right)\right]} \quad (7)$$

In the Langmuir isotherm, K_L (L mg^{-1}) and a_L (L mg^{-1}) were Langmuir constants associated with the affinity of the binding sites. Q_o (mg g^{-1}) = K_L/a_L was the maximum monolayer-adsorption capacity of the adsorbent. In the Freundlich isotherm, n was the heterogeneity factor that reflected the bond energy between the adsorbate and the adsorbent, and K_f was the Freundlich constant indicative of the overall adsorption capacity (mg g^{-1}). In the BET isotherm equation, q_e was the adsorption isotherm capacity (mg/g), and C_{BET} was the BET isothermal constant (L mg^{-1}). Nonlinear regression analysis was performed to align the investigated data and estimate model parameters. A key characteristic of the Langmuir isotherm was the dimensionless constant defined by Equation 8.

$$R_L = \frac{1}{1 + a_L C_0} \quad (8)$$

The R_L value determines the shape of the isotherm, indicating whether it was irreversible ($R_L = 0$), favorable ($0 < R_L < 1$), linear ($R_L = 1$), or unfavorable ($R_L > 1$).

3. Results and Discussion

3.1. CBM Synthesis Products

The observed 11.1% linear shrinkage of the clay honeycomb monolith originates from both moisture removal during air drying and structural rearrangement during calcination at 600°C for 3 h. XRD analysis confirmed that the Sigli (Aceh) clay consists predominantly of SiO_2 (quartz) and $NiSO_4.6H_2O$ (retgersite), which exhibit moderate thermal stability compared with highly swelling clays such as smectites. During air drying, the evaporation of free and capillary water causes particle rearrangement and consolidation, while heating to 600°C promotes further densification by eliminating hydroxyl groups from aluminosilicate phases and burning off residual organics, leading to partial sintering of particle contacts.

For quartz-aluminosilicate clay systems, linear shrinkage values of several percent to ~15% are typically reported under comparable thermal treatments; therefore, the measured value of 11.1% lies within the expected range, indicating controlled consolidation without excessive deformation. The corresponding volumetric shrinkage is approximately 30% $(1-0.889^3) \approx 0.298$, which is relevant to interpreting the changes in porosity, bulk density, and adsorption behavior discussed in subsequent sections. Unlike expandable clays (e.g., montmorillonite), quartz-rich clays typically show lower shrink-swell behavior; therefore, the observed shrinkage is primarily driven by thermal consolidation rather than lattice collapse. When hydroxyl groups are introduced to the clay surface during preparation, clay minerals adsorb these groups by releasing protons [12]. During the preparation of adsorbents, physical activation (calcination) is performed. After the mixing step, the clay swells due to the hydroxyl groups in the solution.

The circular channels in a honeycomb monolith provide smoother fluid flow due to reduced turbulence and drag compared to hexagonal cells, where flow can be disrupted by sharp angles and multiple corners. Circular channels also offer a higher open area for fluid flow by minimizing dead spaces and sharp corners where particles or contaminants might accumulate. Additionally, it is easier to optimize the wall thickness in a circular-cored design to balance mechanical strength and flow area.

3.2. X-ray Diffractometer Analysis

Figure 3 shows the XRD pattern of the CBM after calcination. The diffraction peaks are dominated by sharp quartz (SiO_2), accounting for approximately 87.5 wt%, indicating that the CBM framework is primarily silica-based. Minor crystalline phases such as eucryptite ($LiAlSiO_4$, ~4.8 wt%) are also detected, confirming the presence of residual aluminosilicate components derived from the original clay minerals. The reduced intensity or absence of expandable clay mineral peaks suggests partial dehydroxylation and structural transformation during thermal treatment, resulting in a more rigid ceramic-like monolith structure.

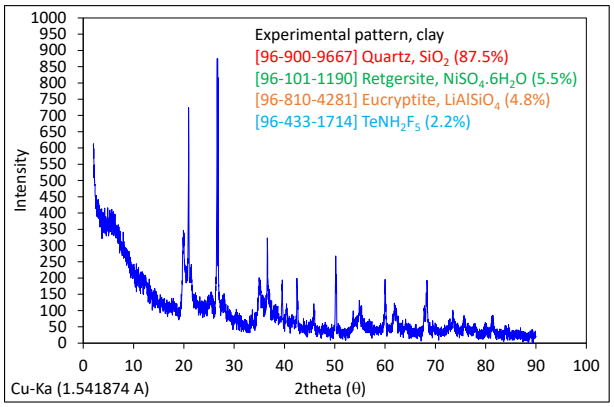

Figure 3. XRD pattern of the clay-based monolith obtained using Cu Kα radiation

Based on a surface chemistry perspective, both SiO_2 and Al_2O_3- phases provide surface hydroxyl groups (≡Si–OH and ≡Al–OH) that control the CBM surface charge. At near-neutral pH, partial deprotonation of these hydroxyl groups results in a negatively charged surface, facilitating Fe^{2+} adsorption via electrostatic attraction and surface complexation. Although quartz is relatively less reactive, the presence of aluminosilicate phases together with the porous monolithic structure observed by SEM enhances the overall adsorption performance.

Therefore, the Fe^{2+} removal in this study results from surface adsorption on mesoporous aluminosilicate domains combined with physical confinement within the porous monolith, rather than from well-ordered clay minerals. The properties specified in the clay mineral composition refer to the arrangement of the basic crystal units, with an average crystal size of 27.25 nm. The Si/Al ratio (greater than 4) suggests high thermal resistance and a hydrophobic surface. This type of adsorbent can be activated by thermal processes, and is suitable for adsorption and catalysts [13].

Clay minerals are particularly attractive because of their abundance, layered structure, and high cation exchange capacity (CEC), enabling metal-ion removal via electrostatic attraction and surface complexation mechanisms [14]. In contrast, silica-dominated Si–O–Si groups are largely inert toward cation adsorption and primarily provide structural stability rather than active binding sites [15]. Consequently, Fe^{2+} uptake by the CBM is mainly associated with alumina-related surface sites, while the high SiO_2 content limits the density of active adsorption centers. The results suggest that Fe^{2+} removal is governed primarily by surface adsorption on mesoporous wall structures rather than interlayer ion exchange, highlighting the influence of mineralogy on adsorption performance.

3.3. Structural and Morphological Analysis

Figure 4 shows SEM images of the CBM at different magnifications. At 7000× (Figure 4a), the monolith walls are composed of irregularly aggregated clay particles forming interconnected interparticle voids. The particle aggregates exhibit non-spherical, plate-like morphology with lateral dimensions in the submicron to micron range, typical of clay-derived aluminosilicate materials.

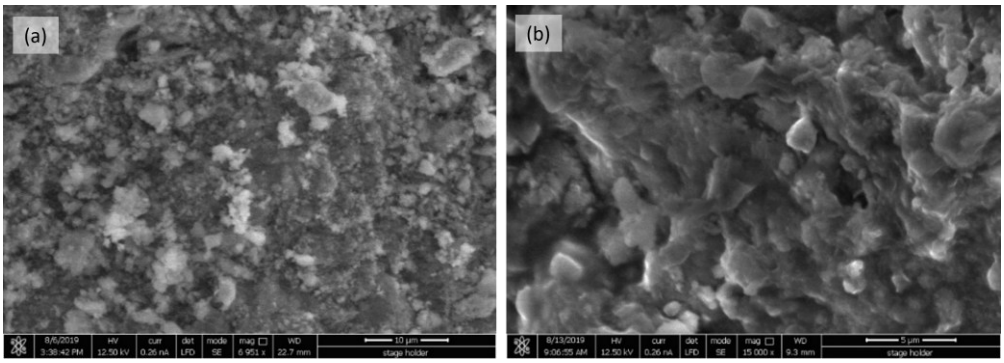

Figure 4. SEM images of CBM at (a) 7000× magnification and (b) 15,000× magnification

At higher magnification (15,000×, Figure 4b), stacked lamellar structures are clearly observed, producing interlayer gaps and fine intra-wall pores. While SEM provides qualitative evidence of pore connectivity and wall roughness, quantitative pore characteristics were determined by N_2 adsorption analysis. The CBM exhibits a dominant mesoporous structure with pore diameters primarily distributed in the range of 7.435–8.689 nm, as derived from the BJH method, and a specific surface area of 55.065 $m^2 g^{-1}$.

The pore structure originates from the intrinsic lamellar arrangement of the raw clay minerals without chemical modification [16]. The combination of lamellar particle morphology, interconnected mesopores, and continuous honeycomb channels is expected to enhance Fe^{2+} adsorption by increasing accessible surface hydroxyl groups (≡Si–OH and ≡Al–OH) and reducing diffusion resistance under continuous-flow conditions. In addition, the continuous, mechanically integrated honeycomb structure supports efficient mass transfer under flow conditions while maintaining a low pressure drop, which explains the favorable adsorption performance of the CBM in continuous-flow Fe^{2+} removal.

3.3.1. Fourier Transfer Infra-Red Analysis

FTIR analysis was performed to characterize the functional groups and mineral structure present in the CBM (Figure 5). The FTIR spectrum exhibits absorption bands at ~3695–3620 cm^{-1} corresponding to Al-OH stretching vibrations, which are characteristic of kaolinite-group minerals, indicating that the original clay mineral structure remained preserved after monolith fabrication.

The band at ~1630 cm^{-1} is assigned to H–O–H bending of physically adsorbed water. The strong band at ~1030 cm^{-1} is associated with Si-O stretching in tetrahedral sheets of aluminosilicate minerals, while bands below 800 cm^{-1} correspond to Si–O–Al and Al–O–Si deformation vibrations. These spectral features are consistent with reference spectra for kaolinite-containing materials, confirming that kaolinite is the dominant clay mineral phase within the CBM. This clay mineral identification in this study is based on FTIR characterization of the monolith itself, rather than the raw clay, while XRD is used to confirm crystalline components such as quartz.

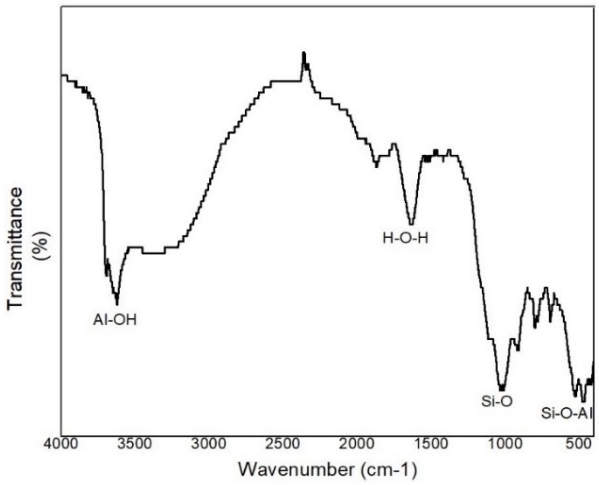

Figure 5. FTIR spectrum of the CBM showing absorption bands associated with kaolinite

FTIR analysis confirmed the presence of hydroxyl bonds, indicating that water is trapped within the clay structure. Silica and alumina are constituted to be major chemicals in the material quantities. The presence of -OH functional groups indicates that SiO_2 still has a hydrophilic nature. The vibration band at 3360 cm^{-1} is specifically associated with the presence of Si-OH groups and molecular water.

3.3.2. Surface Area and Pore Size Distribution

The N_2 adsorption-desorption isotherm of the CBM shows a Type-IV profile with hysteresis (Figure 6), consistent with a mesoporous wall structure (BET area = 55.07 $m^2 g^{-1}$, pore volume = 0.1007 $cm^3 g^{-1}$). A BET of ~55 $m^2 g^{-1}$ is moderate for clay-based materials: kaolinite typically displays low surface areas (often < ~30 $m^2 g^{-1}$), while smectite-rich materials (e.g., montmorillonite or bentonites) commonly show larger values (tens to > 100 $m^2 g^{-1}$ depending on exchange form and treatment). These typical ranges are summarized in the clay mineral review and handbooks [17].

For a monolithic (bulk) form, the measured value is competitive. Monoliths generally exhibit lower apparent BET areas than powders because much of the adsorbent mass is locked into a self-supporting structure (reduced external exposure), yet they gain practical advantages in hydraulic performance and handling. Importantly, adsorption of Fe^{2+} is governed not only by surface area but also by surface chemistry (surface sites, edge/edge-site complexation, and cation-exchange capacity) and pore

accessibility; atomistic and spectroscopic studies show that Fe binds at distinct high- and low-affinity sites on clay edges and that oxidation state/complexation control uptake behavior. Thus, the CBM's hierarchical porosity (microporous channels and mesoporous walls) and the clay mineral functional groups help compensate for a moderate BET surface area and enable measurable Fe^{2+} uptake [18]. Inconsistent fabrication can affect the adsorption performance and overall mechanical stability of the material.

3.4. Pressure Drop

The pressure drop evaluation confirms that the CBM provides a measurable hydraulic advantage over conventional pelletized adsorbents. At a bed height of 40 cm, the CBM produced a pressure drop of 11.16 kPa, compared with 12.65 kPa for pellets. This difference increased at greater heights: at 60 cm, the CBM showed 13.31 kPa versus 16.14 kPa for pellets, and at 100 cm, the CBM reached 18.54 kPa, while pellets exhibited 23.71 kPa. Overall, the CBM reduced pressure drop by approximately 10–20% across the tested bed heights. This trend is consistent with previous findings that monolithic and structured adsorbents typically exhibit lower pressure drops than packed pellets because of their ordered flow channels and reduced tortuosity [19]. The lower hydraulic resistance of the CBM indicates that it can operate with reduced energy consumption and lower blower/compressor demand in fixed-bed adsorption systems. The pellet length is 1 mm, and is considered a short pellet [20].

The pressure-drop behavior of the CBM has important practical implications for continuous-flow water treatment. In filtration and adsorption systems, pressure drop directly determines the pumping energy required to maintain a given flow rate, and excessive hydraulic resistance can significantly increase operational costs and limit system scalability.

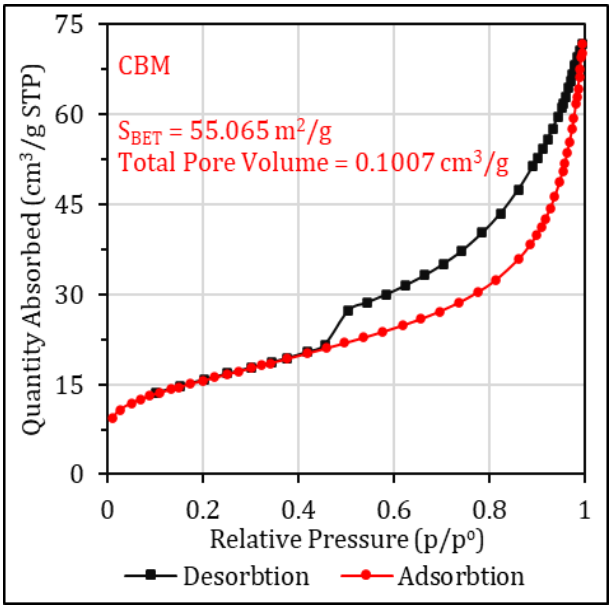

Figure 6. BET isotherm analysis

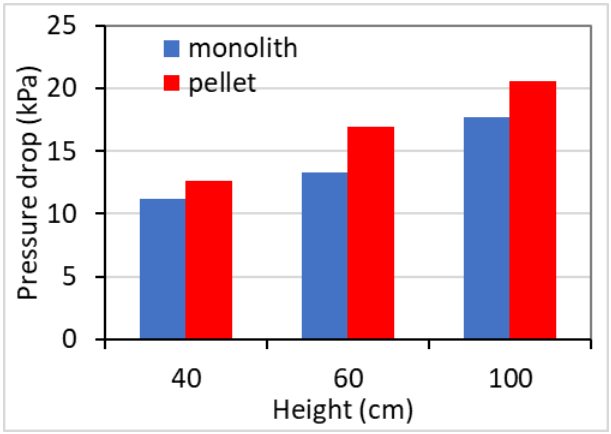

Figure 7. Pressure drops in the adsorber for clay-based adsorbents

As shown in Figure 7, the CBM exhibited a substantially lower pressure drop compared with pellet-type adsorbents at comparable flow conditions. This reduction is attributed to the ordered, parallel macroporous channels of the honeycomb structure, which provide uniform flow pathways and minimize flow tortuosity and channeling. In contrast, packed beds of pellets create irregular interparticle voids that increase flow resistance and are more susceptible to clogging.

Based on an operational perspective, the lower pressure drop of the CBM implies reduced pumping energy requirements, improved hydraulic stability, and longer operational lifetimes before maintenance is required. These advantages are particularly relevant for decentralized or low-resource water treatment systems, where energy efficiency and system robustness are critical design considerations. Importantly, the CBM achieves these hydraulic benefits while maintaining measurable Fe^{2+} adsorption capacity, demonstrating a favorable balance between adsorption performance and hydraulic feasibility.

3.5. Adsorption Kinetics

The adsorption kinetics of Fe^{2+} on CBM were evaluated using both pseudo-first-order and pseudo-second-order models. For both initial Fe^{2+} concentrations (2 and 4 mg L^{-1}), the pseudo-second-order model provided a better fit to the experimental data, as evidenced by higher correlation coefficients (R^2) and lower fitting errors compared to the pseudo-first-order model. In addition, the q_e values predicted by the pseudo-second-order model were in closer agreement with the experimental values (Figure 8 and Table 1).

Although the pseudo-first-order model describes the initial stage of adsorption reasonably well, particularly at short contact times, it fails to adequately represent the overall adsorption behavior over the full-time range. Therefore, the kinetic data indicate that the adsorption process is more accurately described by the pseudo-second-order model, suggesting that the rate-limiting step involves surface interactions between Fe^{2+} ions and adsorption sites on the CBM.

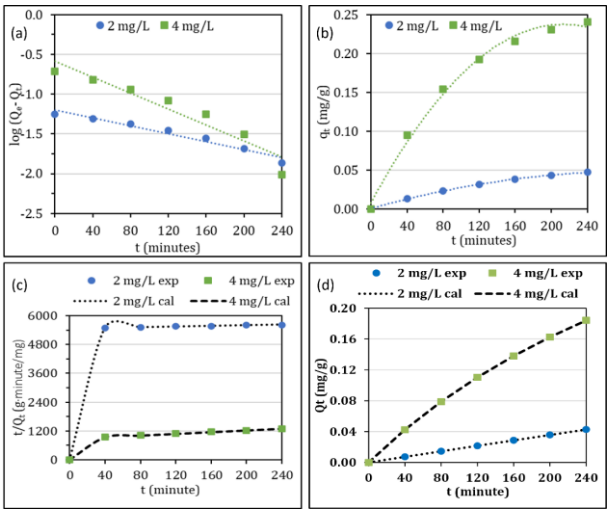

Figure 8. Kinetics of pseudo first order: (a) linear, (b) non-linear, and pseudo second order: (c) linear, (d) non-linear

It should be noted, however, that the superior fit of the PSO model does not by itself confirm chemisorption as the dominant mechanism. Instead, the kinetic behavior reflects the dependence of the adsorption rate on the availability of surface sites, while the overall process may still involve a combination of physical adsorption and surface complexation. The rate constants (k_2) were 0.0001 min^{-1} and 0.0037 min^{-1} at 2 and 4 mg L^{-1} concentrations, respectively.

Initially, abundant active sites on the adsorbent surface led to a rapid increase in adsorbate uptake at the pore sites. As these sites became increasingly occupied, the adsorption rate decreased, and the system gradually approached equilibrium. Although replicate measurements were not conducted, the adsorption data showed smooth and monotonic trends, and the fitted kinetic/isotherm models exhibited high correlation coefficients, indicating internally consistent behavior. Furthermore, the SSE values and the comparison between q_{exp} and q_{cal} in Table 1 demonstrate that the pseudo-second-order model provides the best fit, yielding the lowest SSE.

Adsorption kinetics followed a pseudo-second-order model, indicating that chemisorption is the dominant mechanism [21]. The pseudo-second-order model predicts that the iron ions bind to the surface of the adsorbent with abundant active sites, and the adsorption occurs chemically (chemical adsorption) [22]. This also indicates the sharing of electrons between the binding sites of the adsorbate and adsorbent through covalent bonds. A strong correlation with the kinetic data can effectively explain the adsorption mechanism within the solid phase. In the adsorption process, pseudo-second-order kinetics are more suitable for solutions with low concentrations [23], as in the solutions with relatively low concentrations in this study (2 and 4 mg L^{-1}). The rate constant of 0.0037 min^{-1} (0.22 h^{-1}) implies a faster rate of iron adsorption onto the surface of CBM at environmental temperature levels compared to the rate constant of ethanol adsorption onto the SiO_2/DVB surface.

3.6. Adsorption Isotherm

Figure 9 presents the non-linear plots of the isotherms, while Table 2 summarizes the calculated adsorption parameters and SSE for each isotherm. As indicated in Table 2, all three models produced low SSE values. The Freundlich model resulted in an SSE value of 2.57×10^{-3}, suggesting multisite adsorption on a heterogeneous surface, along with potential interactions among the adsorbed Fe^{2+} ions. The calculated adsorption capacity, k_F, for Fe^{2+} was 0.0572 mg g^{-1}, lower than that of BET (0.077 mg g^{-1}). Additionally, the calculated *n* value for Fe^{2+} was greater than 1, indicating favorable adsorption, driven primarily by physical processes. The error function was an important statistical parameter used to quantify the deviation of the theoretically predicted isotherm parameters and to evaluate the suitability of nonlinear empirical models in research [20].

Table 1. Kinetic parameters for Fe^{2+} adsorption

C_o	Parameter	Pseudo-first-order		Pseudo-second-order	
		Linear	Non-linear	Linear	Non-linear
2 mg L^{-1}	q_e^{exp}	0.0564	0.0564	0.0564	0.0564
	q_e^{cal}	0.0627	0.0500	1.4284	0.0495
	k	0.0057	0.0057	0.0001	0.0001
	SSE	0.0107	0.0003	275.60	0.0000
	R^2	0.9625	0.9995	0.9803	0.9999
4 mg L^{-1}	q_e^{exp}	0.1940	0.1940	0.1940	0.1940
	q_e^{cal}	0.2571	0.2468	0.5572	0.2038
	k	0.0115	0.0115	0.0037	0.0037
	SSE	0.1075	0.0293	0.0951	0.0001
	R^2	0.9119	0.9932	1.0000	0.9998

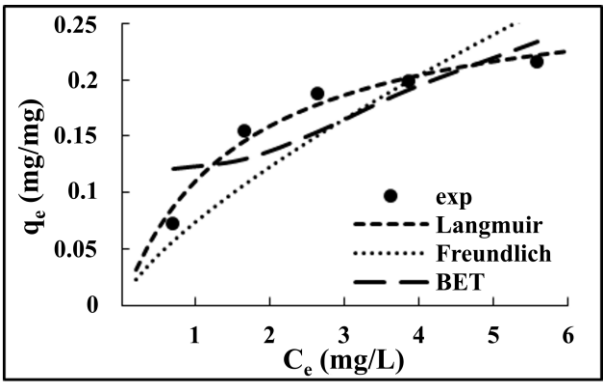

Figure 9. Fe^{2+} adsorption isotherm model

Table 2. Optimal value of the adsorption isotherm

Adsorption isotherm	Isotherm constants	Value
Langmuir	K_L (L mg^{-1})	0.125
	a_L (L mg^{-1})	0.547
	Q_o (K_L/a_L)	0.229
	SSE	1.43×10^{-4}
Freundlich	K_f (mg g^{-1})	0.0572
	n	1.38
	SSE	2.57×10^{-3}
BET	q_s (mg g^{-1})	0.077
	C_{BET} (L mg)	3.21
	SSE	2.01×10^{-3}

Compared with chemically modified clays and functionalized monolith adsorbents reported in the literature, the Fe^{2+} adsorption capacity of the CBM (0.229 mg g^{-1}) is moderate. Modified material typically exhibits higher adsorption capacities because of increased surface charge density or the presence of specific binding sites such as iron oxides or organic functional groups. They typically range from approximately 1 to 20 mg g^{-1} for Fe^{2+} or Fe^{3+} removal under batch conditions [17]. For example, bentonite and zeolite materials have exhibited Fe(III) adsorption capacities in the range of about 9.7–16.7 mg g^{-1} under similar testing conditions (zeolite micro and blue/brown bentonite) in batch studies of Fe(III) removal from aqueous solution, which are one to two orders of magnitude higher than the capacity observed here [24]. Clay minerals such as montmorillonite and kaolinite have also been reported to have significant Fe(III) uptake, with montmorillonite capacities (28.4–28.9 mg g^{-1}) exceeding those of kaolinite (10.4 – 11.2 mg g^{-1}) in comparative studies [16]. However, such powdered materials often exhibit poor hydraulic behavior in continuous-flow systems, including high pressure drop, particle attrition, and the need for post-treatment solid-liquid separation [25].

Compared with unmodified natural clays and ceramic monoliths, the CBM demonstrates competitive adsorption performance while offering superior mechanical integrity, shape stability, and low-pressure drop characteristics under continuous-flow operation. Honeycomb monoliths provide ordered macroporous channels that ensure uniform flow distribution and significantly lower pressure drop than packed beds of pellets or powder [26]. While the measured BET surface area (55 m^2 g^{-1}) is moderate relative to powdered chemically modified clays, it is sufficient to enable measurable Fe^{2+} removal under continuous-flow-relevant conditions. The relatively low adsorption, therefore, represents a trade-off associated with the use of an unmodified natural clay and a monolithic configuration, prioritizing hydraulic efficiency and operational simplicity over a maximum uptake capacity.

Furthermore, the adsorption experiments were conducted at relatively low initial Fe^{2+} concentrations and near-neutral pH, conditions under which Fe hydrolysis and limited driving force for surface binding can occur. The monolithic form also prioritizes hydraulic performance (reduced pressure drop and structural integrity) over maximization of micro- and mesoporosity typical of high-capacity powder adsorbents. Finally, the CBM was used without chemical activation or surface functionalization, unlike many high-capacity adsorbents whose surfaces are modified to introduce specific binding sites.

Similar trade-offs between adsorption capacity and hydraulic performance have been reported for structured adsorbents, where lower equilibrium capacities are compensated by improved mass transfer, reduced pressure drop, and operational simplicity. The results indicate that CBM is better suited for applications requiring stable flow, low energy consumption, and ease of handling, rather than for scenarios where maximum adsorption capacity is the sole performance criterion.

The use of a maximum Fe^{2+} concentration of 9 mg L^{-1} in the adsorption isotherm study is likely intended to reflect conditions commonly found in natural or rural water sources, where iron contaminant typically ranges between 1–10 mg L^{-1}. This concentration range is particularly relevant for applications in household or decentralized water treatment systems, where the primary goal is to reduce Fe^{2+} levels to meet drinking water standards ($\leq$0.3 mg L^{-1}, according to WHO guidelines). Additionally, testing beyond 10 mg L^{-1} could lead to oxidation and precipitation of Fe^{2+} as $Fe(OH)_2$ or $Fe(OH)_3$, which can interfere with adsorption measurements and yield misleading conclusions. The relatively low adsorption capacity of the CBM may also limit its ability to handle high concentrations without reaching saturation too quickly.

Adsorption isotherms are important for designing adsorption processes for industrial implementation, improving industrial implementation, or advancing the evolution of adsorbents [4]. The isothermal study provides original insights into the practical design of the adsorption system, the adsorbent's affinity, surface properties, adsorbent capacity, and the adsorption mechanism. The Langmuir isotherm model predicts that the adsorbent uses a single surface layer during adsorption and that the process is homogeneous. The Freundlich isotherm predicts heterogeneous sites, and that the adsorbent has more than one surface layer (multilayers). The adsorption process, as described by the

BET equation, does not occur solely in a monolayer but also in multilayers, thereby approaching the assumptions of the Freundlich model.

After calculating the SSE for each model, the Langmuir model likely yields the smallest SSE, indicating that it best fits the investigated data. The suitability of the Langmuir isotherm suggests that the adsorption of Fe^{2+} is likely simple and involves a single mechanism. For optimal adsorption, the R_L value should be in the range of $0 < R_L < 1$, as demonstrated in this study. The calculated R_L values ranged from 0.1716 to 0.506, indicating favorable Fe^{2+} adsorption onto CBM. As the initial Fe^{2+} concentration rose from 1.785 to 8.828 mg L^{-1}, the R_L values decreased by over 66%, reflecting improved adsorption favorability.

The Q_0 value from the Langmuir model is lower than that reported by previous researchers [27], but their study used an illite-smectite clay and involved extrusion and a 5 h calcination treatment of CBM to make it waterproof. They reported higher cadmium adsorption capacities for CBM, but their study used a different clay. Specifically, this adsorption capacity was also lower than that of zeolite NaY in HCl adsorption, but it took 40 times less time for CBM to reach breakthrough. Similarly, while certain synthetic mineral adsorbents have shown higher adsorption capacities for metal pollutants than CBM, their production methods are more complex than those of the CBM used in this study.

The pH of the solution plays a crucial role in determining the adsorption of Fe^{2+} ions onto the monolith adsorbent. At low pH levels, the concentration of H^+ ions competes directly with Fe^{2+} for active adsorption sites, resulting in reduced adsorption efficiency. Additionally, the adsorbent surface may become positively charged, further repelling the positively charged Fe^+ ions. As the pH increases to around 5–6, competition with H^+ decreases, and the surface charge of the adsorbent becomes more favorable for attracting metal ions. Within this pH range, Fe^{2+} remains in its dissolved ionic form, allowing for maximum interaction with the adsorbent. However, at pH values above 6, Fe^{2+} tends to form insoluble hydroxide species such as $Fe(OH)_2$ or $Fe(OH)_3$, which precipitate from solution. This not only reduces true adsorption but also complicates interpretation, as removal may be misattributed to adsorption rather than precipitation. Therefore, maintaining an optimal pH is essential to ensure accurate and efficient removal of Fe^{2+} from aqueous solutions using clay-carbon monolith adsorbent.

Nevertheless, this study does not provide a detailed investigation of key adsorption parameters such as pH, temperature, and contact time required to achieve maximum Fe^{2+} removal, all of which can significantly influence adsorption performance under varying environmental conditions. A comprehensive analysis of these parameters, as well as the adaptability of the material for different applications, will be addressed in a separate publication.

The regeneration and reuse of adsorbents are critical for ensuring the economic feasibility and environmental sustainability of water treatment systems. In the case of CBMs, effective regeneration extends the material's service life, reduces operational costs, and minimizes secondary waste. Regeneration typically involves desorbing adsorbed contaminants with chemical agents (e.g., acids, bases, or chelating solutions), followed by rinsing and drying. For Fe^{2+} removal, dilute acid solutions such as 0.1–0.5 N HCl or HNO_3 are often used to protonate the surface and release bound metal ions.

However, the regeneration method must be carefully selected to avoid degrading the structural integrity of the monolith, especially for CBMs that incorporate organic binders such as molasses or biomass-derived carbon. Repeated regeneration cycles may lead to pore collapse, leaching of active components, or fouling by residual organics and inorganics. Nonetheless, studies have shown that with proper optimization. CBMs can retain a significant portion of their adsorption capacity across multiple cycles (e.g., >80% after 3–5 cycles), making them a viable choice for long-term applications [28]. Incorporating regeneration protocols into the design of CBM-based systems not only reduces material consumption but also aligns with circular economy principles and green engineering.

In practical water treatment applications, contaminants commonly coexist; however, the present study evaluates CBMs exclusively under single-solute Fe^{2+} conditions. Consequently, the performance of CBMs in multi-component water matrices was not investigated and cannot be assessed based on the current results. Previous studies have reported that the presence of common background ions (e.g., Ca^{2+}, Mg^{2+}, Na^+) and natural organic matter may influence adsorption behavior on clay-based materials because of competition for adsorption sites or pore blockage [29]. Such effects, however, were not examined in this work and therefore are not discussed further. This lack of selectivity constrains their applicability unless the surface is chemically modified with functional groups (e.g., $-NH_2$ or -COOH) or doped with metal oxides to enhance specificity [30].

The scope of this study is limited to establishing baseline adsorption performance, kinetic behavior, and hydraulic characteristics of CBMs for Fe^{2+} removal in controlled systems. The potential impact of competing ions, anionic species, organic contaminants, or fouling processes remains an important topic for future investigation using well-defined multi-solute experiments. Accordingly, the conclusions drawn here are restricted to single-component systems and to continuous-flow-relevant hydraulic performance.

To assess the practical value of CBMs, it is essential to benchmark their performance against well-established commercial adsorbents such as activated carbon and zeolite. Activated carbon is renowned for its high surface area (800–1500 $m^2\ g^{-1}$) and strong affinity for a wide range of contaminants, including heavy metals. However, its production costs, typically USD 2–5 per kg, and reliance on high-temperature activation processes limit its accessibility in low-resource settings. In

contrast, zeolites offer high cation-exchange capacities and are particularly effective at removing Fe^{2+} and other divalent ions, but they also require mining and purification processes and may be limited in availability in some regions.

CBMs, despite having a relatively low specific surface area (typically < 100 m^2 g^{-1}), offer several advantages, including low raw-material costs, ease of fabrication, and environmental friendliness. For instance, CBMs synthesized from bentonite, biomass-derived carbon, and molasses can be produced at costs below USD 0.5 kg^{-1}. In terms of Fe^{2+} adsorption capacity, CBMs generally exhibit values in the range of 0.2–0.3 mg g^{-1}. Although this capacity is lower than that of activated carbon (0.5–2.0 mg g^{-1}) or synthetic zeolites (1.0–3.0 mg g^{-1}), it remains sufficient for application in large-scale, low-cost water treatment systems [29].

In terms of regeneration, activated carbon often undergoes structural degradation and pore collapse after multiple chemical or thermal cycles, whereas zeolites may exhibit ion-exchange fatigue over time. CBMs, on the other hand, have shown acceptable regeneration performance, retaining >80% of their adsorption capacity after 3–5 acid-washing cycles, with minimal loss of structural integrity when operated under moderate conditions [28]. While CBMs may not match the efficiency of advanced materials, their simplicity, low cost (Table 3), and sustainability make them a practical alternative in decentralized or rural water treatment systems where affordability and local material use are prioritized.

The durability of CBM in wet, flow-through environments is a critical factor in its real-world applicability. In continuous-flow systems, CBMs are exposed to prolonged saturation and hydraulic pressure, which may lead to deformation, swelling, or loss of mechanical integrity. These effects are particularly pronounced in monoliths that rely on organic binders, such as molasses or carbon precursors, which may degrade or leach over time. Standardized tests such as ASTM C1424, the uniaxial compressive strength test, and ASTM D4644, the slake durability test, can be used to evaluate the monolith's resistance to mechanical stress and water-induced degradation. Modifications such as incorporating mineral additives (e.g., silica, fly ash) or thermal curing have been shown to significantly improve wet compressive strength. For instance, monoliths reinforced with silica fume retained up to 78% of their dry strength after water immersion. These enhancements are vital to prevent structural collapse or channeling during operation and must be optimized for reliable, long-term use in water treatment columns or filter cartridges.

CBMs are 2–4 times cheaper than activated carbon or zeolite (Table 4). All primary materials (bentonite, molasses, and coconut charcoal) are widely available in rural or agricultural regions, making local production feasible. The cost per treated volume of water remains low because of reusability (3–5 cycles). This cost model supports the claim of economic viability for CBMs in decentralized, low-income water treatment settings.

Table 3. Theoretical cost breakdown for 1 kg of CBM (Note: Cost values are theoretical estimates based on laboratory-scale experience, local material prices, and internal calculations. Actual costs may vary depending on scale and location)

Component	Estimated cost per kg or L	Quantity per kg CBM	Estimated cost (USD)	Notes
Bentonite clay	$0.05 – 0.10/kg	0.6 kg	$0.03–0.06	Readily available in most regions
Coconut shell charcoal	$0.20–0.50/ kg (raw)	0.25 kg	$0.05 – 0.13	Locally produced biochar
Molasses (binder)	$0.20–0.40/L	0.15 L	$0.03–0.06	Byproducts from sugar industries
Water (mixing)	Negligible	~0.5 L	-	Locally sourced
Fuel (drying/firing)	$0.10–0.20/unit	0.3 unit	$0.03–0.06	Local biomass LPG
Labor (manual, rural)	$3.00–5.00/day	~0.2 day/kg	$0.60–1.00	Varies by region
Equipment depreciation	-	-	$0.02–0.05	Assumes reuse of molds, kiln

Table 4. Comparison to commercial adsorbents (Note: Cost values are theoretical estimates based on laboratory-scale experience, local material prices, and internal calculations. Actual costs may vary depending on scale and location)

Material	Cost (USD/kg)	Fe^{2+} capacity mg g^{-1}	Regenerable	Notes
CBM (this study)	~$1.00	~0.2–0.3	Yes (acid wash)	Low-cost, locally sourced
Activated carbon	$2.00–5.00	0.5–2.0	Limited	Expensive, energy-intensive
Zeolite (natural)	$1.50–3.00	0.8–2.5	Yes (exchange)	More selective, higher cost

4. Conclusion

Clay-based honeycomb monoliths (CBMs) were successfully synthesized and evaluated as structured adsorbents for Fe^{2+} removal from water. XRD analysis indicates that the monolith consists mainly of SiO_2 and $NiSO_4.6H_2O$-based clay minerals, which provide negatively charged surface sites suitable for Fe^{2+} ions. The CBMs exhibit hierarchical porosity, with mesoporous walls supplying adsorption sites and ordered macroporous channels ensuring low hydraulic resistance. The BET surface area (~55 $m^2\ g^{-1}$) is typical of natural clays and enables measurable Fe^{2+} uptake. Adsorption kinetics at 2 and 4 mg L^{-1} are better described by the pseudo-second-order model, indicating that surface-site interactions govern the overall uptake process. Equilibrium data follow the Langmuir isotherm, yielding a maximum adsorption capacity of 0.229 mg g^{-1}. Although this capacity is lower than that of chemically modified clay adsorbents, it reflects the use of unmodified natural clay and a monolithic design optimized for mechanical stability and hydraulic performance rather than maximum uptake. Pressure-drop measurements confirm that CBMs exhibit substantially lower hydraulic resistance than pellet-type adsorbents, supporting their suitability for continuous-flow operation with reduced energy demand. Overall, CBMs are best positioned as hydraulically efficient and structurally robust pre-treatment or polishing adsorbents. Future work should focus on capacity enhancement through surface modification, clarification of adsorption mechanisms using post-adsorption spectroscopy, and evaluation under competitive-ion and long-term flow conditions. In addition, competitive-ion experiments and long-term continuous-flow tests should be conducted to assess CBM performance under realistic groundwater conditions and evaluate operational stability.

Acknowledgement

This research is fully supported by Process Technology Laboratory USK. The authors fully acknowledged financial support from the Ristekdikti, and the Institute for Research and Community Service of Universitas Syiah Kuala through the Senior Lecturer Grant No. 74/UN11.2/PP/PNBP/SP3/2019.

References

[1] Naomi Carrard, Tim Foster, Juliet Willetts, Groundwater as a Source of Drinking Water in Southeast Asia and the Pacific: A Multi-Country Review of Current Reliance and Resource Concerns, *Water*, 11, 8, (2019), 1605 https://doi.org/10.3390/w11081605

[2] World Health Organization, *Guidelines for Drinking-Water Quality: Fourth Edition Incorporating the First and Second Addenda*, World Health Organization, 2022,

[3] Claudia Fujita, M. Shahbaz Akhtar, Ray Hidaka, Makoto Nishigaki, Mitigation of groundwater iron-induced clogging by low-cost bioadsorbent in open loop geothermal heat pump systems, *Applied Water Science*, 12, 3, (2022), 30 https://doi.org/10.1007/s13201-022-01574-x

[4] Mirna Lubis, Dwinta Fujianti, Rita Zahara, Darmadi Darmadi, The Optimization of the Electrocoagulation of Palm Oil Mill Effluent with a Box-Behnken Design, *International Journal of Technology*, 10, 1, (2019), 291-319 https://doi.org/10.14716/ijtech.v10i1.838

[5] Muhammad Ibrahim, Muhammad Haq Nawaz, Prangya Ranjan Rout, Jun-Wei Lim, Bandita Mainali, Muhammad Kashif Shahid, Advances in Produced Water Treatment Technologies: An In-Depth Exploration with an Emphasis on Membrane-Based Systems and Future Perspectives, *Water*, 15, 16, (2023), 2980 https://doi.org/10.3390/w15162980

[6] Nitha Abraham, Jency James, Tuhin Banerji, Ratish Menon, Development of a novel groundwater iron removal system using adsorptive Fe(II) process, *Groundwater for Sustainable Development*, 10, (2020), 100318 https://doi.org/10.1016/j.gsd.2019.100318

[7] Ismi Nurul, Syamsuddin Yanna, Adisalamun Adisalamun, Aulia Sugianto Veneza, Darmadi Darmadi, Adsorption of Iron (II) Ion by Using Magnetite-Bentonite-Based Monolith from Water, *Key Engineering Materials*, 892, (2021), 10-16 https://doi.org/10.4028/www.scientific.net/KEM.892.10

[8] Valentina Stampi-Bombelli, Alba Storione, Quirin Grossmann, Marco Mazzotti, On Comparing Packed Beds and Monoliths for CO_2 Capture from Air Through Experiments, Theory, and Modeling, *Industrial & Engineering Chemistry Research*, 63, 26, (2024), 11637-11653 https://doi.org/10.1021/acs.iecr.4c01392

[9] Félix Sumariva, F. Javier Moreno-Dorado, Francisco M. Guerra, Daniel Goma, Hilario Vidal, José Manuel Gatica, Use of clay honeycomb monoliths for the removal of tetracycline antibiotic from water, *Journal of Water Process Engineering*, 68, (2024), 106381 https://doi.org/10.1016/j.jwpe.2024.106381

[10] Meifeng He, Wenbin Hu, A study on composite honeycomb sandwich panel structure, *Materials & Design*, 29, 3, (2008), 709-713 https://doi.org/10.1016/j.matdes.2007.03.003

[11] M. P. Yeste, J. M. Gatica, M. Ahrouch, H. Vidal, Clay honeycomb monoliths as low cost CO_2 adsorbents, *Journal of the Taiwan Institute of Chemical Engineers*, 80, (2017), 415-423 https://doi.org/10.1016/j.jtice.2017.07.031

[12] Neeraj Kumari, Chandra Mohan, Basics of Clay Minerals and Their Characteristic Properties, in: G.M. Do Nascimento (Ed.) *Clay and Clay Minerals*, IntechOpen, London, 2021, https://doi.org/10.5772/intechopen.97672

[13] P. Suarya, Karakterisasi Adsorben Komposit Aluminium Oksida pada Lempung Teraktivasi Asam, *Jurnal Kimia*, 6, 1, (2012), 93-100

[14] Garrison Sposito, *The Chemistry of Soils*, 3rd ed., Oxford University Press, New York, 2016,

[15] Donald L. Sparks, *Environmental Soil Chemistry*, 2nd ed., Academic Press, San Diego, 2003,

[16] Narcisse Dobe, Daouda Abia, Constant Tcheka, Jean Paul Nongni Tejeogue, Massai Harouna, Removal of amaranth dye by modified Ngassa clay: Linear and non-linear equilibrium, kinetics and statistical

study, *Chemical Physics Letters*, 801, (2022), 139707 https://doi.org/10.1016/j.cplett.2022.139707

[17] Krishna Gopal Bhattacharyya, Susmita Sen Gupta, Adsorption of a few heavy metals on natural and modified kaolinite and montmorillonite: A review, *Advances in Colloid and Interface Science*, 140, 2, (2008), 114-131 https://doi.org/10.1016/j.cis.2007.12.008

[18] Annamária Kéri, Rainer Dähn, Maria Marques Fernandes, Andreas C. Scheinost, Matthias Krack, Sergey V. Churakov, Iron Adsorption on Clays Inferred from Atomistic Simulations and X-ray Absorption Spectroscopy, *Environmental Science & Technology*, 54, 19, (2020), 11886-11893 https://doi.org/10.1021/acs.est.9b07962

[19] Berend Smit, Jeffrey R. Reimer, Curtis M. Oldenburg, Ian C. Bourg, *Introduction to Carbon Capture and Sequestration*, Imperial College Press, London, 2014,

[20] Darmadi Darmadi, Mahidin Mahidin, Siti Syifa Azzahra, Munadiya Masrura, Adsorption of Mercury(II) Ion in Aqueous Solution by Using Bentonite-Based Monolith, *Key Engineering Materials*, 885, (2021), 77-84 https://doi.org/10.4028/www.scientific.net/KEM.885.77

[21] Tawfik A. Saleh, Chapter 2 - Adsorption technology and surface science, in: T.A. Saleh (Ed.) *Interface Science and Technology*, Elsevier, 2022, https://doi.org/10.1016/B978-0-12-849876-7.00006-3

[22] Jianlong Wang, Xuan Guo, Adsorption kinetic models: Physical meanings, applications, and solving methods, *Journal of Hazardous Materials*, 390, (2020), 122156 https://doi.org/10.1016/j.jhazmat.2020.122156

[23] Jay C. Bullen, Sarawud Saleesongsom, Kerry Gallagher, Dominik J. Weiss, A Revised Pseudo-Second-Order Kinetic Model for Adsorption, Sensitive to Changes in Adsorbate and Adsorbent Concentrations, *Langmuir*, 37, 10, (2021), 3189-3201 https://doi.org/10.1021/acs.langmuir.1c00142

[24] Tomáš Bakalár, Mária Kaňuchová, Anna Girová, Henrieta Pavolová, Rudolf Hromada, Zuzana Hajduová, Characterization of Fe(III) Adsorption onto Zeolite and Bentonite, *International Journal of Environmental Research and Public Health*, 17, 16, (2020), 5718 https://doi.org/10.3390/ijerph17165718

[25] K. Y. Foo, B. H. Hameed, Insights into the modeling of adsorption isotherm systems, *Chemical Engineering Journal*, 156, 1, (2010), 2-10 https://doi.org/10.1016/j.cej.2009.09.013

[26] T. A. Nijhuis, M. T. Kreutzer, A. C. J. Romijn, F. Kapteijn, J. A. Moulijn, Monolithic catalysts as more efficient three-phase reactors, *Catalysis Today*, 66, 2, (2001), 157-165 https://doi.org/10.1016/S0920-5861(00)00621-0

[27] Mohammadi Ahrouch, José Manuel Gatica, Khalid Draoui, Dolores Bellido-Milla, Hilario Vidal, Clay honeycomb monoliths for the simultaneous retention of lead and cadmium in water, *Environmental Technology & Innovation*, 27, (2022), 102765 https://doi.org/10.1016/j.eti.2022.102765

[28] Jenifer Gómez-Pastora, Eugenio Bringas, Inmaculada Ortiz, Recent progress and future challenges on the use of high performance magnetic nano-adsorbents in environmental applications, *Chemical Engineering Journal*, 256, (2014), 187-204 https://doi.org/10.1016/j.cej.2014.06.119

[29] T. A. H. Nguyen, H. H. Ngo, W. S. Guo, J. Zhang, S. Liang, Q. Y. Yue, Q. Li, T. V. Nguyen, Applicability of agricultural waste and by-products for adsorptive removal of heavy metals from wastewater, *Bioresource Technology*, 148, (2013), 574-585 https://doi.org/10.1016/j.biortech.2013.08.124

[30] Yanbo Zhou, Jian Lu, Yi Zhou, Yongdi Liu, Recent advances for dyes removal using novel adsorbents: A review, *Environmental Pollution*, 252, (2019), 352-365 https://doi.org/10.1016/j.envpol.2019.05.072